Identification of a Resonant Imaging Process in Apertureless Near-Field Microscopy

H.-T. Chen and S. Kraatz
Department of Physics, Rensselaer Polytechnic Institute, Troy, New York 12180, USA

G. C. Cho
IMRA America, 1044 Woodridge Ave., Ann Arbor, Michigan 48105, USA

R. Kersting*
Department of Physics, University of Munich, 80779 Munich, Germany
(Received 29 August 2003; published 21 December 2004)

We report on apertureless near-field microscopy in the far infrared. We identify a configurational resonance of the scanning tip-surface system to be the dominating mechanism that forms the image. Experimental data such as the high imaging contrast and its spectral properties can be well explained and make the framework of a mesoscopic resonance an alternative to conventional scattering models that are used to interpret near-field data. Our findings are plausibly not restricted to the far infrared and may impact on near-field spectroscopy in general.

DOI: 10.1103/PhysRevLett.93.267401 PACS numbers: 78.47.+p, 07.57.–c, 07.79.Fc

The development of the scanning near-field optical microscope (SNOM) has revolutionized optical imaging and led to applications ranging from biophysics to optical data storage [1,2]. Spatial resolutions down to 10 Å have been achieved using apertureless SNOMs, where a nanometer-size scanning tip provides the resolution [3,4]. Today, most apertureless SNOMs operate in the visible region of the spectrum and first attempts have been undertaken to access the near-infrared and midinfrared ranges in order to image the vibrational resonances of the specimen [5]. Further developments towards far-infrared wavelengths hold promise, for instance, for mapping of biological cells and for semiconductor device inspection, where nanometer resolutions may enable tracing of charge carrier distributions in submicron devices. Despite such stimulating opportunities for applications, the development of apertureless SNOMs for the far infrared is challenging. A frequently cited concept for the physics of apertureless SNOMs is that of a Mie scatterer, which probes the near field by diffuse scattering [2,6]. However, in the far infrared Mie scattering becomes inefficient. The cross sections for scattering and absorption scale down with $1/\lambda^4$ and $1/\lambda$, respectively [6]. Thus, demonstrations of far-infrared near-field imaging as described in Refs. [7,8] indicate that processes other than Mie scattering are involved and that the general understanding of apertureless near-field imaging is far from complete. This is supported by the progress achieved by theoretical works on near-field physics. Methods such as finite-difference time-domain techniques, discrete dipole approximation techniques, or Green dyadic techniques allow going beyond the approximation of a pointlike Mie scatterer and taking into account the mesoscopic properties of the imaging system [9,10]. Configurational resonances similar to those of antenna systems [11] are expected to occur in near-field imaging [12,13].

Several works have addressed near-field imaging in the far infrared using THz techniques and resolutions of several micrometers were achieved using aperture filtering techniques [14–16]. Recently, apertureless THz imaging with 10 μm resolution was reported [7,17] and our group demonstrated a THz-SNOM with 150 nm resolution [8]. We observed an image contrast that exceeded those values, which were expected from conventional scattering theory by orders of magnitude. Thus, a refined understanding and the identification of the physical process behind it is required. In this Letter, we exclusively analyze the underlying physics of apertureless imaging in the far infrared and identify a mechanism, which results from a mesoscopic resonance and makes imaging with nanometer resolution possible. We will show by time-resolved THz experiments that imaging is dominated by an ac coupling between incident light field and the tip-surface system. The imaging process distinguishes from that expected from conventional scattering theory by its signal strength, spectral dependence, and optical phase of the image-giving THz signal. Although our experimental work exclusively addresses the far-infrared range, it can be extrapolated that the observed ac coupling may play a dominant role in other spectral ranges such as the near infrared and maybe even in the visible. Independent of whether the field of application is in biology or semiconductor device inspection, the ac coupling mechanism affects significantly the interpretation of microscopic images, when physical properties such as the dielectric function of a surface are deduced.

The THz-SNOM experiments are performed in a geometry as illustrated in Fig. 1. Few-cycle THz pulses are focused onto the sample to a spot diameter $D \approx 4\lambda$, which is given by the numerical aperture of the focusing optics. The angle of incidence is about 60° and the electric field is p-polarized. At the THz spot the electric field is

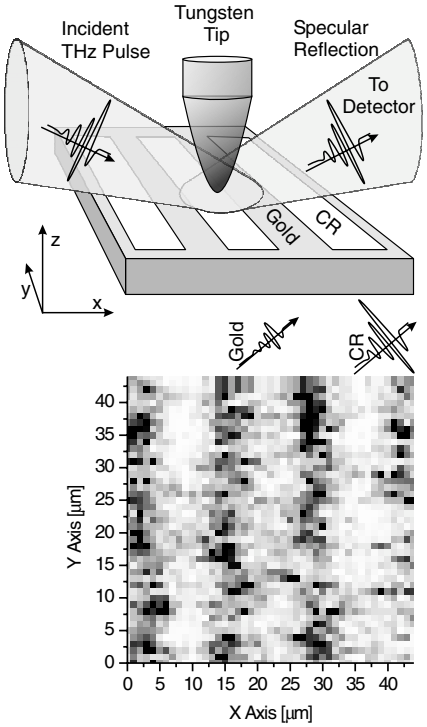

FIG. 1. Schematic of microscope head and sample. The THz beam is focused to the diffraction limit onto the surface, where the tip scans the near field. Only the specular reflection of the THz radiation is detected. The lower part shows a THz image of a CR grating with 14 μm period that was fabricated on a gold surface. High amplitudes of the specularly reflected THz field are shown by white dots.

sampled by a tungsten probe, which has a tip radius of 1 μm, a cone angle of 16°, and an overall length $l \gg D$. The THz radiation is generated by femtosecond laser excitation of n-doped InAs. The center frequency of the few-cycle THz pulses is about 2.0 THz, which corresponds to 150 μm wavelength. In order to prevent absorption by atmospheric humidity, the experiments are performed in a vacuum chamber where the water partial pressure is less than 30×10^{-3} mbar. A more detailed description of the spectroscopic specifications can be found in Refs. [18,19]. After transmission through the microscope head, the THz pulses are time resolved by electro-optic sampling [20]. What distinguishes our geometric configuration from most SNOM geometries is that the specularly reflected beam is detected and not the scattered signal. This allows us to measure the relation between incident and reflected light. Furthermore, our time-resolved THz experiments map the electric field of the beam. This provides direct information about both the spectral amplitude distribution and the optical phase of the detected signal and allows us to draw a complete picture of the physical processes that are involved in near-field imaging.

The lower part of Fig. 1 shows a THz image of an organic grating, which consists of 350 nm thick lines of cresol resin (CR) compound with $\epsilon \approx 1.36$ on top of a gold layer. The image was recorded at zero time delay, when the incident THz pulse has its maximum field strength. During imaging, the tip was held at a constant height of 400 nm above the gold surface, which corresponds to 50 nm above the CR. The 14 μm period of the structure can be clearly resolved. A spatial resolution of about 2 μm is achieved. Taking into account the thickness of the CR lines, we deduce that our technique can detect volumes as small as 1.4×10^{-18} m^3. Spatial resolutions down to 150 nm were achieved with a probe of 100 nm tip radius when the distance between tip and structure is reduced [8]. It is important to compare the experimental findings with the basic concept of Mie scattering in order to make clear the necessity for a novel physical framework that goes beyond the concept of a pointlike scatterer. Two properties of our experimental data were unexpected: (i) An image contrast of 0.2% is deduced when comparing the field amplitudes, which were recorded above the gold and the CR. This exceeds the expected values due to scattering by about 2 orders of magnitude. (ii) The fact that higher signals of the specularly reflected beam are measured above the CR lines. It should be emphasized that in all experiments the tip is held at constant height with respect to the gold surface. The electric field lines that are induced by the THz radiation below the tip are grounded in the metal surface. Thus, in terms of physical properties, above the CR lines only the dielectric constant of the tip-surface system is increased. In this case, an enhanced loss of the specularly reflected field due to scattering would be expected according to the standard model [2,6]. Our results clearly show the opposite (see Fig. 1). The phenomenon is not material specific. It was observed on all organic as well as inor-

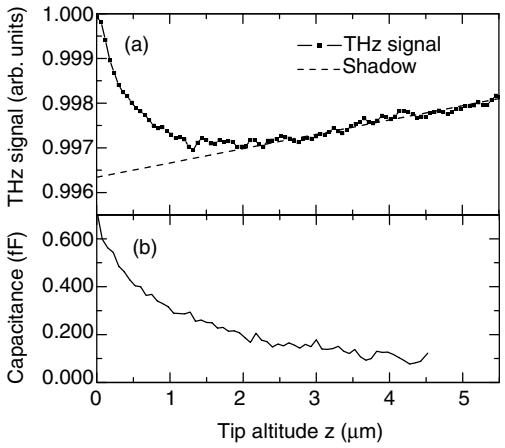

FIG. 2. Dependence of (a) THz signal and (b) capacitance on the altitude of the tip above the gold surface. The THz data were recorded at zero time delay, which corresponds to the temporal maximum of the THz pulse.

ganic structures we investigated. Furthermore, completely different results are obtained when deducing dielectric constants from the image data. According to the scattering model an increased specular reflection indicates a reduced dielectric constant [2,5,6], while our data shows that the opposite is the case. The above findings contradict the exclusive validity of the scattering concept and indicate that a yet unreported mechanism dominates image formation.

In order to understand the mechanism that allows for near-field detection, we will focus in the following on measurements, which are performed on a plain metal surface. Figure 2(a) shows the dependence of the specularly reflected THz field on the distance z between tip and gold surface. Approaching the tip towards the surface leads to a decreasing THz signal, which is due to diffraction losses when the tip moves into the THz beam and casts a shadow. However, at distances smaller than 1.5 μm the detected signal increases again. It is this increase, which gives the image contrast in apertureless THz near-field microscopy. An understanding of the underlying physics can be deduced from the dependence of the capacitance of the tip-surface system on the tip altitude z, which reveals a strong increase on the same distance scale [Fig. 2(b)]. In the following, we will show that this increase in capacitance affects a nearly resonant ac coupling of the tip-surface system and allows for THz imaging with nanometer resolution.

Time-domain measurements give more insight into the underlying physics, because both the spectral distribution of field amplitudes as well as their optical phases can be deduced. Figure 3(a) shows the incident THz pulse and the differential signal, which was obtained by measuring the signal difference between tip altitudes of 0.1 and 1.6 μm, respectively. The corresponding amplitude spectrum consists mostly of low frequency components [Fig. 3(b)]. Additionally, we found that the optical phase of the differential signal is zero with respect to the incident THz pulses. Both findings contrast the model of a light scattering tip-surface system. In this framework one would expect a spectral frequency dependence of ν^n with $n = 1, 4$ and a phase shift of π, which is associated with the signal loss due to scattering.

In the following, we will develop a model, which addresses the dielectric properties of the tip-surface system. We will consider exclusively the mesoscopic properties, i.e., those that appear in the near-field region of the scanning system. The background is that the tip-surface system has a resonance at $\nu_{\mathrm{res}} = 1/2\pi\sqrt{LC}$ in case of negligible damping. We deduced $\nu_{\mathrm{res}} \approx 0.5$ THz using the capacitance C as deduced from our measurements and an inductance $L = 0.3$ nH. This value is typical for a conical monopole with a length $l \approx 2\lambda$, as given by the illumination of the tip within the THz spot. In terms of these quantities, the relation between the power, which is dissipated by the tip-surface system, and the incident THz power is given by

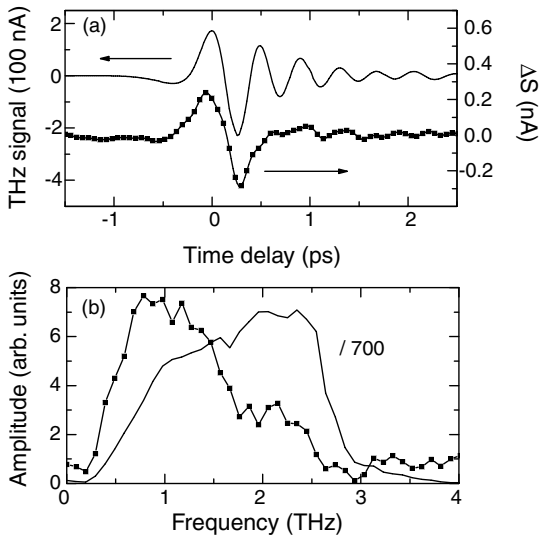

FIG. 3. (a) Time-domain measurements of the incident THz pulse (solid line) and the differential signal ΔS (symbols), which is the difference between the signals obtained at tip altitudes of 0.1 and 1.6 μm, respectively. (b) Corresponding amplitude spectra of incident signal and differential signal, where the incident spectrum has been divided by a factor of 700.

$$\eta = \frac{P_{\mathrm{diss}}}{P_{\mathrm{inc}}} = \frac{RZ_0}{4\pi[R^2 + (\omega L - \frac{1}{\omega C})^2]} \tag{1}$$

where Z_0 is the vacuum impedance and R is the input resistance, which describes the energy loss of the dipole due to Ohmic dissipation as well as by emission into the semisphere around the tip [21]. In our experiments, the electric field is measured and the normalized image contrast of the electrical field amplitude due to dissipation is $\Delta E/E_{\mathrm{inc}} = \frac{1}{2}\Delta\eta$, where $\Delta\eta$ refers to changes of the power dissipation.

Figure 4(a) shows the dependence of the dissipation loss η for two tip altitudes. The dashed line illustrates a calculation for a capacitance of 250 aF, which is our experimental value for a distance of 1.6 μm. Bringing the scanning tip closer to the surface (0.1 μm) increases the overall capacity of the system to about 600 aF (see Fig. 2), thus lowering the resonance frequency (solid curve in Fig. 4(a). However, both resonances lie below the spectrum of the incident THz pulse. This causes a reduced overall dissipation loss—i.e., an increased field amplitude of the specular reflection—when the tip approaches the surface. The same happens when the dielectric constant between tip and surface is increased. The resulting spectral change is compared to the experimental data in Fig. 4(b). A sound agreement is achieved when using an input resistance R of about 1000 Ω, which is reasonable for systems of several wavelengths scale [21].

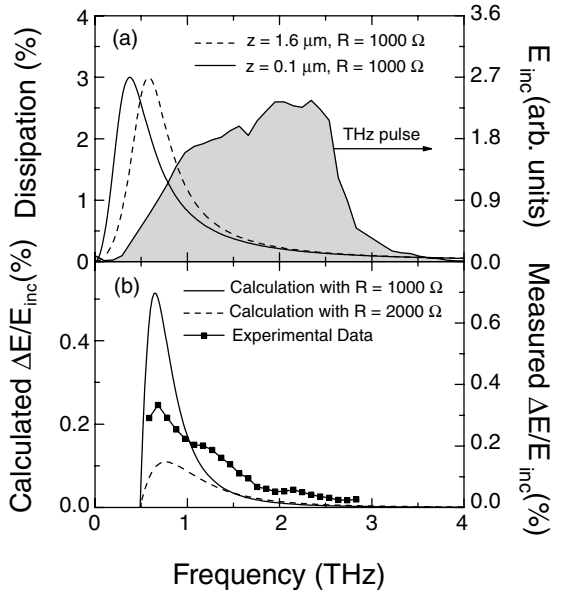

FIG. 4. (a) Calculated loss spectra for tip altitudes of 0.1 μm (solid line) and 1.6 μm (dashed line). The gray shaded curve illustrates the spectrum of the incident THz field. (b) Corresponding differential signal and experimental data. Two calculations are shown, which base on an input resistance of $R = 1000\ \Omega$ (solid line) and $R = 2000\ \Omega$ (dashed line), respectively.

Both experimental as well as calculated data show a frequency dependence that clearly distinguishes from the ν^n dependence of the standard scattering model. Additional confirmation for our approach comes from the spectrally integrated changes of 0.16%, which are in reasonable agreement with the observed 0.12% as deduced from Fig. 3(b).

We conclude that ac coupling of the tip-surface system is the dominant mechanism that allows for near-field microscopy in the far infrared. However, ac coupling may play an important role at much higher frequencies, provided that the geometry of the tip is scaled with wavelength. Because the tip radius can be as small as several nanometers [4], resonantly enhanced losses may play an important role in nanoscale imaging in the near infrared and maybe even in the visible.

In summary, we found that configurational resonances dominate optical near-field imaging in the far infrared. The resonances result from the mesoscopic properties of the tip-surface system and lead to an efficient ac coupling between light field and scanning tip. The concept that imaging results from a resonance distinguishes it from the commonly used framework to interpret the scanning system as a scatterer by an unique spectral dependence and optical phase of the image contrast. Both properties lead to significant differences when the dielectric constant of a surface is deduced from image data. We expect that the mechanism may also have a relevant contribution in other spectral ranges and that it may impact further understanding of near-field microscopy and the interpretation of image data.

The authors thank G.-C. Wang and X.-C. Zhang for helpful discussions. This research was supported by NSF (ECS02-45461), Semiconductor Research Corporation (2001-RJ-971G), and the Army Research Office (DAAD190210255).

*Electronic address: roland.kersting@physik.uni-muenchen.de
URL: http://www.thz.physik.uni-muenchen.de

[1] E. Betzig, J. Trautman, T. Harris, J. Weiner, and R. Kostelak, Science **251**, 1468 (1991).
[2] *Near-Field Nano/Atom Optics and Technology*, edited by M. Ohtsu (Springer, New York, 1998).
[3] J. Wessel, J. Opt. Soc. Am. B **2**, 1538 (1985).
[4] F. Zenhausern, Y. Martin, and H. Wickramasinghe, Science **269**, 1083 (1995).
[5] B. Knoll and F. Keilmann, Nature (London) **399**, 134 (1999).
[6] C. Bohren and D. Huffman, *Absorption and Scattering by Small Particles* (John Wiley & Sons, New York, 1983).
[7] K. Wang, A. Barkan, and D. Mittleman, in *Technical Digest of Conference of Lasers and Electro-Optics (CLEO2003), Baltimore, MD, USA, 2003* (Optical Society of America, Washington, DC, 2003).
[8] H.-T. Chen, R. Kersting, and G. C. Cho, Appl. Phys. Lett. **83**, 3009 (2003).
[9] B. T. Draine and P. J. Flatau, J. Opt. Soc. Am. A **11**, 1491 (1994).
[10] C. Girard and A. Dereux, Rep. Prog. Phys. **59**, 657 (1996).
[11] K. Crozier, A. Sundaramurthy, G. Kino, and C. Quate, J. Appl. Phys. **94**, 4632 (2003).
[12] M. Xiao, S. Bozhevolnyi, and O. Keller, Appl. Phys. A **62**, 115 (1996).
[13] J. Porto, P. Johansson, S. Apell, and T. Lopez-Rios, Phys. Rev. B **67**, 085409 (2003).
[14] S. Hunsche, M. Koch, I. Brener, and M. Nuss, Opt. Commun. **150**, 22 (1998).
[15] O. Mitraofanov, M. Lee, J. Hsu, I. Brener, R. Harel, J. Federici, J. Wynn, L. Pfeiffer, and K. West, IEEE J. Sel. Top. Quantum Electron. **7**, 600 (2001).
[16] Q. Chen, Z. Jiang, G. X. Xu, and X.-C. Zhang, Opt. Lett. **25**, 1122 (2000).
[17] N. van der Valk and P. Planken, Appl. Phys. Lett. **81**, 1558 (2002).
[18] A. Filin, M. Stowe, and R. Kersting, Opt. Lett. **26**, 2008 (2001).
[19] R. Ascazubi, O. Akin, T. Zaman, R. Kersting, and G. Strasser, Appl. Phys. Lett. **81**, 4344 (2002).
[20] Q. Wu, M. Litz, and X.-C. Zhang, Appl. Phys. Lett. **68**, 2924 (1996).
[21] W. L. Stutzman and G. A. Thiele, *Antenna Theory And Design* (John Wiley and Sons, New York, 1998), 2nd ed.